Graphene-Based Sensor for Low Stain Sensing Applications

MD ABDULLAH AL MAMUN[1,2], LEANDRO MAIO[1],
MD RAJU AHMED[1,2], ANURA FERNANDO[1]
and PRASAD POTLURI[1,2]

[1]Department of Materials, University of Manchester, M13 9PL, Manchester, UK
[2]Northwest Composite Centre, The University of Manchester, M13 9PL, Manchester, UK

Abstract

The innovation and application of advanced functional materials have significantly contributed to the development of sensors for structural health monitoring (SHM)-oriented applications, paving the way for a new era of intelligent structures. Graphene-based sensors have emerged as highly promising owing to their remarkable mechanical, thermal, and electrical properties. Such sensors offer high sensitivity, excellent stretchability, and multifunctional capabilities for detecting various structural parameters. This work explores the development and characterisation of graphene ink films for low-strain sensing applications. Conductive graphene ink films are fabricated using the electrospinning technique. The morphology, electrical properties, and gauge factor of the films are investigated. The effect of strain rate variation on the sensing performance is also investigated. The gauge factor ranges from 10.2 to 11.3 under every condition. Additionally, cyclic bending tests confirm the repeatability and stability of the sensors, demonstrating minimal signal drift and consistent gauge factor performance across loading cycles. The results indicate that graphene ink films offer an easy, power-efficient, weightless and non-intrusive solution for low-strain sensing with potential applications in areas such as SHM and wearable electronics.

Keywords: sensors, graphene ink, sensor film, monitoring

1. Introduction

Advanced functional material-based sensors represent a recent trend in structural health monitoring (SHM) applications. Researchers are utilising new technologies to fabricate sensors that possess high sensitivity while being less intrusive to the host structure. Among these techniques, screen printing[1], [2], [3], [4], inkjet printing [5], 3D printing [6], [7], [8] laser-induced method [9] and vapour deposition [10], [11] are the most common methods. Though some of the reported sensors have high sensitivity, fabrication and scalability limit their implementation. Graphene-based sensors have emerged as highly promising due to their remarkable capabilities for detecting various structural parameters [12], [13]. Researchers have been exploring the incorporation of conductive graphene ink in the fabrication of highly sensitive sensors for SHM applications. Besides advantages, the proposed approaches have some limitations, for instance, they need extra time and temperature for curing. In addition, the hysteresis effect of the graphene materials affects the durability and repeatability of the sensors. Moreover, very few studies investigated linear sensor performance below 0.1% of strain [7], [14]. Despite some studies that have reported sensing performance for the lower strain, the sensitivity is low. For instance, Zitoun A. et al.

investigated the gauge factor at low strain and reported lower and nonlinear sensitivity [12]. They found the gauge factor around 6 in the linear region.

Electrospinning has the potential for sensor fabrication, enabling the production of thin films and the uniform distribution of particles across the film [15], [16]. Additionally, this method eliminates the need for an extra curing process. This study focuses on the development of an electrospun graphene-based sensor that functions at a lower strain. For this, a conductive graphene ink is prepared and after optimisation, the ink is printed onto a polyimide tape (Kapton) and then attached to the aluminium substrate to assess the sensing performance. The performance of the developed sensor was investigated by a cantilever bending test. Results indicated that the sensor demonstrated considerable sensitivity at lower strains.

2. Materials and Methods

2.1 Materials

For Ink preparation, an amine functionalised Graphene (Aminated graphene oxide, Tapped Density = 0.45 g cm^{-3}, supplied by Adnano Technologies Ltd) was used. Polycaprolactone (Mw~14,000, density 1.146 g/mL at 25 °C) and Dimethylformamide (ACS reagent, ≥99.9%) were supplied by Sigma Aldrich. A Kapton film of 25 microns was used as the printing substrate. An aluminium (Al) flat sheet was utilised as the test substrate. The Al specimen was 50 mm wide, 1.5 mm in dimension, with a 70 GPa Young's modulus. The copper tape and conductive silver paste were employed to construct the connection.

2.2 Ink Preparation and optimisation

A schematic representation of the graphene ink preparation process is provided in Figure 1.

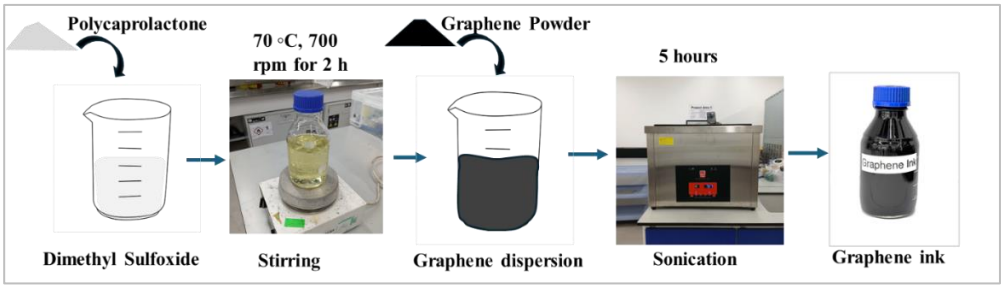

Figure 1. Schematic representation of the stepwise preparation process of the graphene-based conductive ink.

The concentration percentage of graphene is optimised by measuring the initial resistance, change in resistance of the printed substrate and observing the stability of the sensor response.

2.3 Initial Resistance Measurement and Ink Characterisation

This study optimised the graphene content percentage by varying it to 4%, 5%, and 6% of the developed ink. For this, the ink is applied layer-by-layer to the Kapton substrate using the doctor blade method. The initial resistance was measured after every layer of coating using a digital multimeter. The graphene ink was characterised using Fourier Transform Infrared (FTIR) spectroscopy (Bruker Optics, UK). The surface morphology of the sensing layers was examined using a Quanta 250 Scanning Electron Microscope (FEI Company, OR, USA) to evaluate the microstructural features and distribution of the graphene network.

2.4 Sensor Fabrication

The electrospinning technique is employed to print graphene onto the Kapton substrate (Figure 2). Table I presents the machine's parameters. Two sets of specimens are prepared using a 5% concentration of graphene while varying the time or number of sprays. Table II illustrates the characteristics of the fabricated sensor films.

Table I Electrospinning process parameters.

Solutions	Voltage (KV)	Flow Rate (ml//hr)	Working Distance (cm)	Needle Gauge (Number of Needles/Inch)	Collector Speed (rpm)
Graphene Ink	21	5	20	18	250

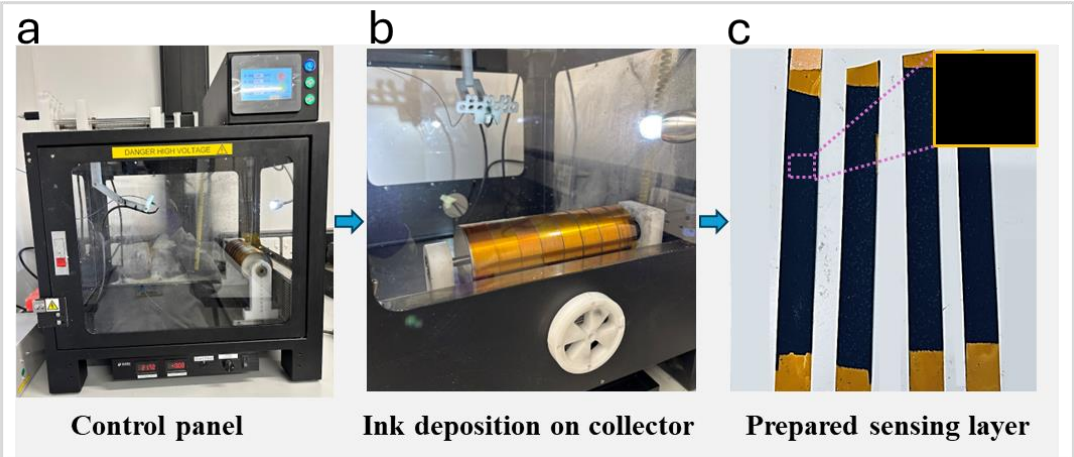

Figure 2. a) Electrospinning setup used for depositing graphene ink onto Kapton substrate, b) Formation of nanofibrous sensing layer on rotating collector, c) Printed sensor films.

Table II specifications of the electro-spun sensor films.

Sample Name	Time (Minutes)	No of Sprays	Dimension (Length × Width)	Thickness (µm)	Graphene Content (g)	Initial Resistance (Ω)
Sample-1	175	43,750	10 mm x 10 mm	81	0.018	2850
Sample-2	280	70,000	10 mm x 10 mm	113	0.0033	1950

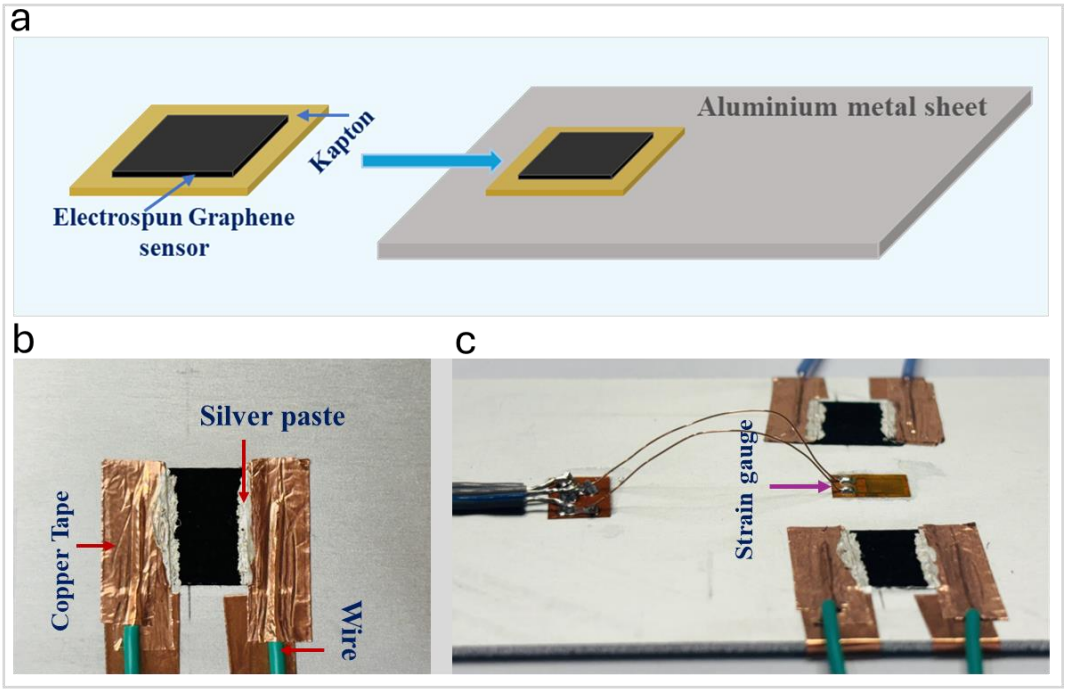

Figure 3. a) Schematic of sensor attachment on aluminium beam, b) Application of copper tape and silver paste for electrode connection, and c) Final installed sensor system on aluminium substrate.

2.5 Fabrication of the sensing layer with Electrodes

Since the sensor films are required to be attached to the testing substrate, the electro-spun sensor films are cut using a laser machine with dimensions of 10 mm x 10 mm in length and width accordingly. After this, the Kapton film with graphene printed sensor is attached to the surface of the aluminium specimen (Figure 3).

2.6 Electromechanical Test

This study aimed to evaluate the electromechanical response of the sensing films by analysing the variation in electrical resistance under static loading conditions, thereby assessing their strain sensitivity. Therefore, a cantilever bending test is conducted to examine both tension and compression. To conduct the mechanical

testing, a universal testing machine (Instron 5969, Model B11590, Norwood, MA, USA) equipped with a 10 N load cell was utilised. Figure 4 presents the experimental setup of the test. To record the change in resistance of the graphene-based films, these are connected to LabVIEW (Version: 2023, Q3) software (NI-9219).

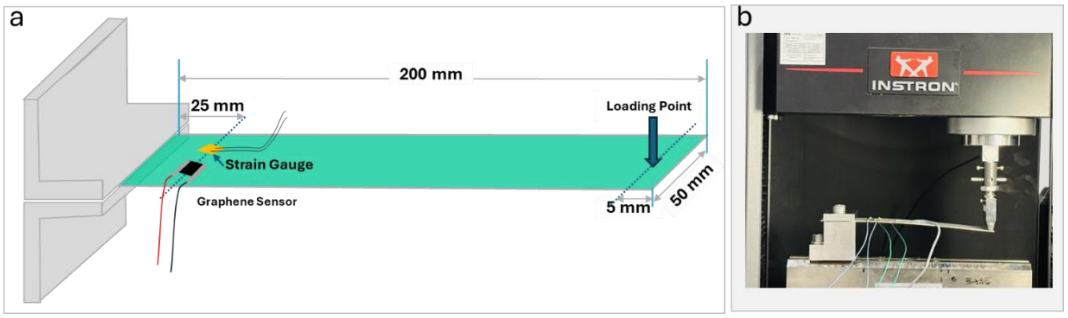

Figure 4. a) Schematic of the cantilever bending test setup and b) Experimental arrangement for electromechanical testing under static loading.

3. Results and Discussion

3.1 FTIR Spectroscopy Analysis

Upon incorporation of graphene into the PCL and DMF mixture, the FTIR spectrum of the ink demonstrated a notable shift of the N–H bending vibration from 1585 cm^{-1} to approximately 1539 cm^{-1}. Additionally, the C–N stretching region (around 1086 cm^{-1}) exhibited broadening and slight intensity changes compared to the individual components. These spectral changes suggest the occurrence of intermolecular interactions between the amine groups of graphene and the carbonyl groups of both PCL and DMF, primarily through hydrogen bonding. The ester C=O peak at 1727 cm^{-1} and the amide C=O peak at 1660 cm^{-1} remained present without significant new peak formation, indicating that the interaction is physical in nature rather than covalent chemical bonding.

3.2 Morphological Investigation

Optical images and SEM analysis were performed to assess the surface texture and structural porosity of the sensing layer. Figure 5 displays the images of the sensor film fabricated using the electrospinning method. The distribution of graphene particles across the surface appeared to be mostly uniform throughout the sensing film. Furthermore, a nanofibrous structure is evident on the surface of the specimen.

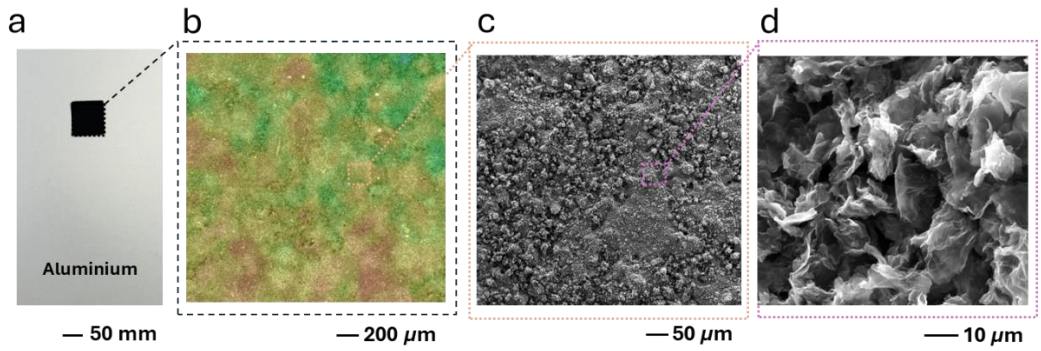

Figure 5. Film morphology of the electro-spun graphene-based sensing layer, (a) Photographs of sensors fabricated on aluminium substrate, (b-c) Optical micrographs of surface texture, (d) SEM image highlighting fibrous morphology and graphene dispersion.

3.3 Bending Tests

The strain sensing was performed by conducting cantilever bending at a constant rate of 2 mm/min (Setup 1). The test parameter is shown in Figure 6a. Figure 6b reveals that both samples exhibit an unmistakable piezoresistive bending response, with Sample 2 displaying an enhanced peak resistance variation. Figure 6c, further demonstrates that Sample 2 is more electromechanically sensitive under similar loading conditions. A greater $\Delta R/R_0\%$ points towards Sample 2 possessing a more loosely dispersed or fine network structure, which allows for more efficient strain transduction. The sensitivity calculated (gauge factor) of both samples, as indicated in Figure 6d, conforms to this finding. Sample 2 exhibits a gauge factor higher than 10, while Sample 1 stays below 9.

To assess the strain rate dependence, sensors were measured at 2, 5, and 10 mm/min under identical bending (Figure 7). At every rate, an increase in resistance with strain is observed, though at higher speeds, strain sensitivity slightly drops. The respective $\Delta R/R_0\%$ curves for Sample 1 at every strain rate are provided in Figure 7b, revealing that maximum change in resistance slightly drops as strain rate increases, a sign of viscoelastic lag or compromised efficiency in strain transfer at higher deformations. The calculated gauge factor behaviors at different strain rates for Sample 1 are provided in Figure 7c. There is a slight dip in sensitivity with speed, as there is a transient misalignment of applied mechanical strain and reorganisation of conductive network.

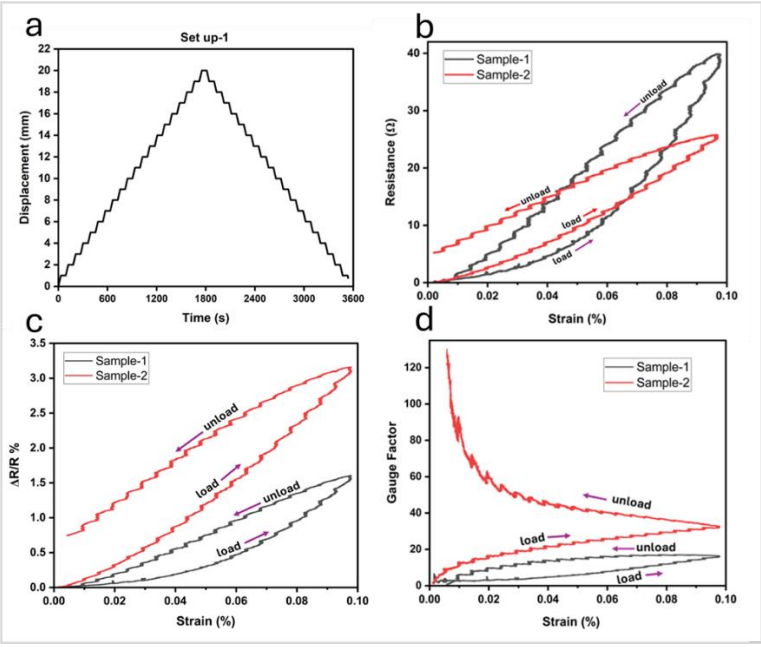

Figure 6. a) Test parameter for setup-1; test results for both samples, b) strain versus change in resistance, c) strain versus ΔR/R%, d) sensitivity of the sensor.

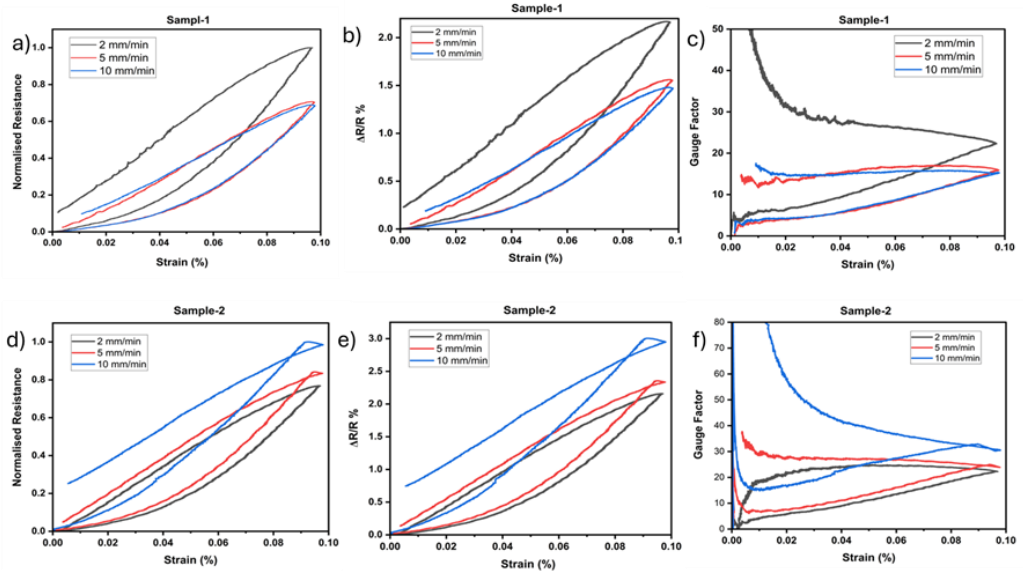

Figure 7. a) Normalised resistance vs strain at different speeds (Sample 1), b) ΔR/R% at different speeds (Sample 1), c) Sensitivity at different speed (Sample 1), d) Normalised resistance vs strain at different speed (Sample 2), e) ΔR/R% at different speeds (Sample 2).

In Figure 7d, Sample 2 evidences more pronounced and linearly rising normalised resistance with strain at every speed, with negligible deviation among the curves. In Figure 7e, $\Delta R/R_0\%$ values remain high at every speed, showing a lesser decline compared to Sample 1. Sample 2 is noteworthy for retaining strong electromechanical sensitivity even at 10 mm/min, enhancing its durability to dynamic deformation. The gauge factor (sensitivity) trend of Sample 2 shows

improved strain-rate independence compared to Sample 1. The values range from 10.2 to 11.3 under every condition, attesting to a more sensitive and mechanically flexible conducting network.

The resultant gauge factor and normalised resistance change differences observed in Sample 1 and Sample 2 can be further explained by analysis of underlying material properties. The electrical sensitivity of these graphene sensors is strongly dependent upon flake orientation, percolation network structure, and mechanical flexibility. Sample 2's better performance at higher strain rates indicates more ideal percolative network structure and reduced junction resistance variation. The role of strain rate in signal attenuation may be explained by dynamic mechanical incompatibility and time-dependent viscoelastic behavior of substrates. At larger deformation speeds, it is common for polymer matrices to experience inefficient stress transfer owing to delayed molecular reorientation.

4. Conclusion

This study presents the successful fabrication and characterisation of a graphene-based electrospun sensor proficient in detecting low-strain deformations with enhanced sensitivity. Two sets of specimens were fabricated with two different thicknesses with optimised concentration percentage of graphene. Bending test was performed for two setups. The sensors demonstrated a gauge factor between 10.2 and 11.3 across different strain rates, surpassing previously documented low-strain sensors. Given its ease of fabrication, eliminating separate curing process and high sensitivity within 0.1% strain regions, the proposed graphene-based strain sensor holds significant promise for real-time monitoring in aerospace, civil infrastructure, and wearable systems. For future optimisation, finite element modeling (FEM) could be applied to simulate strain distribution and optimise sensor placement for maximum signal fidelity. Moreover, future study may focus on hysteresis analysis of the sensor and investigate the sensitivity applying dynamic strain.

Acknowledgements

The authors gratefully acknowledge funding from Commonwealth Scholarship Commission (CSC) U.K. for a Ph.D. scholarship for Md. Abdullah Al. Mamun. This study is supported by the CSC, UK.

References

[1] Q. Wang *et al.*, 'An embedded non-intrusive graphene/epoxy broadband nanocomposite sensor co-cured with GFRP for in situ structural health monitoring', *Compos. Sci. Technol.*, vol. 236, p. 109995, May 2023, doi: 10.1016/j.compscitech.2023.109995.

[2] B. Hao *et al.*, 'Screen-Printed Transparent Flexible Sensors for Liquid Solvent Detection', *ACS Appl. Electron. Mater.*, vol. 6, no. 6, pp. 4167–4177, Jun. 2024, doi: 10.1021/acsaelm.4c00271.

[3] N. Anderson, N. Szorc, V. Gunasekaran, S. Joshi, and G. Jursich, 'Highly sensitive screen printed strain sensors on flexible substrates via ink composition optimisation', *Sens. Actuators Phys.*, vol. 290, pp. 1–7, May 2019, doi: 10.1016/j.sna.2019.02.028.

[4] X. Gong, K. Huang, Y.-H. Wu, and X.-S. Zhang, 'Recent progress on screen-printed flexible sensors for human health monitoring', *Sens. Actuators Phys.*, vol. 345, p. 113821, Oct. 2022, doi: 10.1016/j.sna.2022.113821.

[5] P. Zhou *et al.*, 'An inkjet-printed, flexible, ultra-broadband nanocomposite film sensor for *in-situ* acquisition of high-frequency dynamic strains', *Compos. Part Appl. Sci. Manuf.*, vol. 125, p. 105554, Oct. 2019, doi: 10.1016/j.compositesa.2019.105554.

[6] I. L. Hia, A. D. Snyder, J. S. Turicek, F. Blanc, J. F. Patrick, and D. Therriault, 'Electrically conductive and 3D-printable copolymer/MWCNT nanocomposites for strain sensing', *Compos. Sci. Technol.*, vol. 232, p. 109850, Feb. 2023, doi: 10.1016/j.compscitech.2022.109850.

[7] M. F. Hassan *et al.*, 'Wireless Printed Large-Area Sensors for Continuous Structural Health Monitoring', *Adv. Mater. Technol.*, vol. 10, no. 5, p. 2401782, 2025, doi: 10.1002/admt.202401782.

[8] D. Maurya *et al.*, '3D printed graphene-based self-powered strain sensors for smart tires in autonomous vehicles', *Nat. Commun.*, vol. 11, no. 1, p. 5392, Oct. 2020, doi: 10.1038/s41467-020-19088-y.

[9] A. M. Barja *et al.*, 'Laser-Induced Graphene Strain Sensors for Body Movement Monitoring', *ACS Omega*, vol. 9, no. 37, pp. 38359–38370, Sep. 2024, doi: 10.1021/acsomega.3c09067.

[10] Y. He, K. Luo, X. Zhang, T. Wu, and Q. Wang, 'Transfer-free preparation of flexible strain sensors using high quality VGNs', *Sens. Actuators Phys.*, vol. 366, p. 114949, Feb. 2024, doi: 10.1016/j.sna.2023.114949.

[11] V. Yokaribas, S. Wagner, D. S. Schneider, P. Friebertshäuser, M. C. Lemme, and C.-P. Fritzen, 'Strain Gauges Based on CVD Graphene Layers and Exfoliated Graphene Nanoplatelets with Enhanced Reproducibility and Scalability for Large Quantities', *Sensors*, vol. 17, no. 12, Art. no. 12, Dec. 2017, doi: 10.3390/s17122937.

[12] A. Zitoun *et al.*, 'Graphene-based strain sensing in composites for structural and health monitoring applications', *SN Appl. Sci.*, vol. 4, no. 2, p. 58, Jan. 2022, doi: 10.1007/s42452-022-04940-1.

[13] M. Nie, Y. Xia, and H. Yang, 'A flexible and highly sensitive graphene-based strain sensor for structural health monitoring', *Clust. Comput.*, vol. 22, no. 4, pp. 8217–8224, Jul. 2019, doi: 10.1007/s10586-018-1727-9.

[14] J. Neilson, P. Cataldi, and B. Derby, 'Graphene-Based Transparent Flexible Strain Gauges with Tunable Sensitivity and Strain Range', *ACS Appl. Nano Mater.*, vol. 6, no. 23, pp. 21763–21774, Dec. 2023, doi: 10.1021/acsanm.3c03967.

[15] T. M. Brugo *et al.*, 'Self-sensing hybrid composite laminate by piezoelectric nanofibers interleaving', *Compos. Part B Eng.*, vol. 212, p. 108673, May 2021, doi: 10.1016/j.compositesb.2021.108673.

[16] S. Lotfian, C. Giraudmaillet, A. Yoosefinejad, V. K. Thakur, and H. Y. Nezhad, 'Electrospun Piezoelectric Polymer Nanofiber Layers for Enabling in Situ Measurement in High-Performance Composite Laminates', *ACS Omega*, vol. 3, no. 8, pp. 8891–8902, Aug. 2018, doi: 10.1021/acsomega.8b00940.